applied sciences

MDPI

Article

Use of Nanoparticles as Nanoelectrodes in Contact-Less Cell Membrane Permeabilization by Time-Varying Magnetic Field: A Computational Study

Emma Chiaramello [1,*], Serena Fiocchi [1], Marta Bonato [1], Silvia Gallucci [1,2], Martina Benini [1,2] and Marta Parazzini [1]

[1] Consiglio Nazionale delle Ricerche (CNR), Istituto di Elettronica e di Ingegneria dell'Informazione e delle Telecomunicazioni (IEIIT), Piazza L. da Vinci, 32, 20133 Milano, Italy; serena.fiocchi@ieiit.cnr.it (S.F.); marta.bonato@ieiit.cnr.it (M.B.); silvia.gallucci@ieiit.cnr.it (S.G.); martina.benini@ieiit.cnr.it (M.B.); marta.parazzini@ieiit.cnr.it (M.P.)

[2] Dipartimento di Elettronica, Informazione e Bioingegneria (DEIB), Politecnico di Milano, Piazza L. da Vinci, 32, 20133 Milan, Italy

* Correspondence: emma.chiaramello@ieiit.cnr.it

Abstract: This paper describes a computational approach for the assessment of electric field enhancement by using highly conductive gold nanoparticles (Au NPs) in time-varying electromagnetic fields cell membrane permeabilization, estimating the influence of the presence of Au NPs on transmembrane potential and on the pore opening dynamics. To account for variability and uncertainty about geometries and relative placement and aggregations of the Au NPs, three different NP configurations were considered: spherical Au NPs equally spaced around the cell; cubic Au NPs, for accounting for the possible edge effect, equally spaced around the cell; and spherical Au NPs grouped in clusters. The results show that the combined use of Au NPs and a time-varying magnetic field can significantly improve the permeabilization of cell membranes. The variability of NPs' geometries and configurations in proximity of the cell membrane showed to have a strong influence on the pore opening mechanism. The study offers a better comprehension of the mechanisms, still not completely understood, underlying cell membrane permeabilization by time-varying magnetic fields.

Keywords: contact-less cell permeabilization; gold nanoparticles; time-varying magnetic fields; computational modeling

Citation: Chiaramello, E.; Fiocchi, S.; Bonato, M.; Gallucci, S.; Benini, M.; Parazzini, M. Use of Nanoparticles as Nanoelectrodes in Contact-Less Cell Membrane Permeabilization by Time-Varying Magnetic Field: A Computational Study. *Appl. Sci.* **2021**, *11*, 11121. https://doi.org/10.3390/app112311121

Academic Editor: Vitalij Novickij

Received: 11 October 2021
Accepted: 19 November 2021
Published: 23 November 2021

1. Introduction

The use of electric fields to increase the permeability of biological membranes to molecular species is known as electroporation [1]. One of the most commonly accepted explanation about the mechanism underlying electroporation is that due to the presence of a high-amplitude electric field in proximity of the membrane, the transmembrane potential changes, causing repulsion and dislocation of the phospholipids, which contributes to the development of pore formation in the membrane and makes it partially permeable, allowing the transport of molecules [1]. As it is possible to achieve membrane permeabilization for every cell or tissue type, electroporation could enable a wide range of applications, including delivery of chemotherapeutic drugs [2,3], immunotherapy of cancer and neurodegenerative diseases [4], and genetic transfection, e.g., for RNA and DNA vaccination [5,6].

Due to the wide range of possible applications, many different electroporation protocols and stimulation strategies have been developed to improve the efficacy of the treatment. However, all electroporation protocols require direct contact between the electrodes and the tissues, suffering from the drawbacks common to all invasive procedures and making it difficult to use the technique for a broad range of treatments. Moreover, the application of electric pulses can show other drawbacks, such as the presence of electro-chemical reactions

in the electrode–electrolyte interfaces [7] or the possible electrical breakdown between the electrodes [8].

An alternative approach to achieving membrane permeabilization is the use of time-varying magnetic fields (Pulsed Electromagnetic Fields (PEMF)) [9–14]. This is a completely contactless technique, thus avoiding the use of electrodes, with many advantages such as lower costs and less patient discomfort, allowing the use of the techniques in a wide range of treatments. Studies using PEMF in vitro [9–13] and in vivo [14–17] have demonstrated that PEMF allows permeabilizing the cell membrane, but the efficiency is much lower than that achieved by the conventional electroporation approach. This is because the amplitude of the electric field induced by PEMF in proximity of the cell membrane is almost two orders of magnitude lower that the one obtained by classical electroporation techniques [18,19].

A possible strategy to overcome this issue is to exploit the conductive properties of metal nanoparticles—such NPs, acting as nanoelectrodes, would enhance the induced electric field locally, i.e., close to the membrane, thus potentially enabling cell permeabilization. It was recently proved that the addition of highly conductive gold NPs (Au NPs) in conventional electroporation protocol local enhanced the induced electric field, leading to significant cellular permeabilization [18]. Thanks to the local enhancement of the electric field, the presence of Au NPs was found to also ameliorate the complete coverage of the sample in terms of uniformity and intensity of the electric field [20]. Moreover, the presence of Au NPs should cause membrane permeabilization over nanoscale regions without affecting the entire membrane, thus avoiding collateral damage. Improvements of conventional electroporation protocols by addition of Au NPs has been already observed experimentally in vitro by showing increased mammalian cells transfection [21,22] and efficiency in anticancer therapy [22]. Moreover, two recent studies aimed to obtain a better comprehension of the phenomenon [23,24] by the numerical assessment of the local enhancement of the electric field due to Au NPs using different conventional electroporation protocols.

Regarding the use of Au NPs in contactless permeabilization by time-varying magnetic fields, a first in vitro attempt was described in [18], assuming that the Au NPs could act as nanoelectrodes, locally enhancing the electric field amplitude to the levels known to allow permeabilizing the cell membrane in conventional electroporation protocols. The results described in [18] showed that the combined use of Au NPs and PEMF enhanced the permeabilization of both CHO cells and Gram-negative bacteria, with no effect on survival. However, apart from these experimental findings, no numerical assessment and model of the nanoparticles placed in time-varying electromagnetic fields was described in the literature.

This study focused on filling this research gap: using a computational approach, the numerical assessment of the electric field enhancement by using Au NPs placed in time-varying electromagnetic fields was carried out. The experimental set-up described in [18] was modelled, and the influence of the presence of Au NPs on the transmembrane potential were investigated. To account for the uncertainty about the positions, the geometry, and the aggregation of Au NPs around the cell membrane, different conditions including spherical NPs, cubic NPs, and aggregated of NPs were simulated. Using a spherical cell model and a pore dynamics model, the influence of the position and shape of the Au NPs, as well as the distance from the HI-PEMF source on the pore opening mechanism was assessed.

Such an assessment, quantifying amplitude and localization of the enhancement of the electric field due to the presence of the Au NPs, could help in giving a better comprehension about the mechanisms, still not completely understood, underlying cell membrane permeabilization by time-varying magnetic fields. This contribution could potentially enable the use of a contact-less cell permeabilization technique offering important improvements compared to the existing protocols based on conventional electroporation.

2. Materials and Methods

2.1. Simulated Experimental Set-Up

Figure 1 shows the geometry of the source of the time-varying magnetic field, consisting of a circular coil with a radius equal to 3.07 mm, in which a time-varying electric current flows (Figure 1a). The biological cell and the Au NPs were assumed to be positioned in the hole at the center of the coil, surrounded by extracellular medium. The magnetic pulse was approximated as a sinusoid with frequency equal to 33 kHz and amplitude 5.5 T.

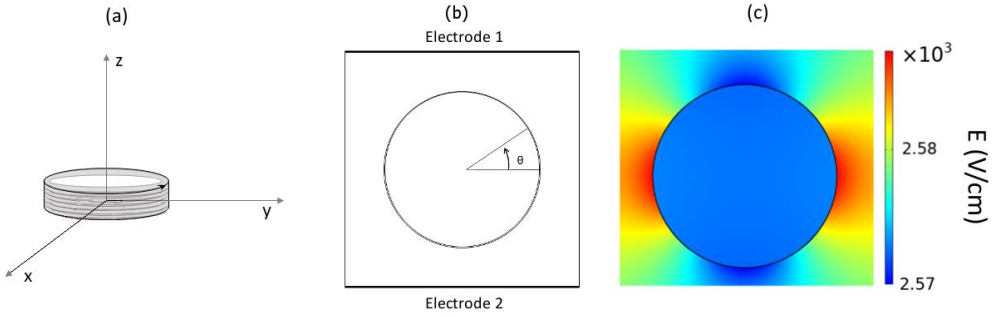

Figure 1. Schematic view of the 3D geometry of the source of the time-varying magnetic field (**a**), of the 2D geometry (**b**), and of the spherical cell placed in an extra-cellular medium and the 2D electric field distribution (**c**).

The cell was modeled by a three-layered spherical model, composed of three homogenous and isotropic regions: the extracellular medium (0#), the membrane (1#), and the intracellular cytoplasm (2#). The external cell radius and membrane thickness were set equal to 10 µm and 10 nm, respectively, while dielectric permittivity ε and conductivity σ values in the three cell regions are reported in Table 1.

Table 1. Dielectric properties of cell regions.

	ε (F/m)	σ (S/m)
Extracellular medium	5.93×10^{-10}	0.55
Membrane	1.035×10^{-10}	1.26×10^{-7}
Cytoplasm	5.93×10^{-10}	0.55

The Au NPs were modeled as solids with conductivity equal to 4.11×10^7 S/m. Two geometries were simulated: spherical NPs with a radius equal to 40 nm, similarly to the approach described in [23], and cubic NPs with a side length equal to 40 nm, in order to take into account the irregular shape of real-life nanoparticles, which cause enhancement of the localized field, known as the edge effect [25].

Three different conditions, simulating different relative positions of the Au NPs around the cell placed and shown in Figure 2, were considered: (1) 24 Au NPs were placed all around the cell, on the $z = 0$ plane, at a radial distance from the membrane equal to 20 nm and with an angular distance among them equal to 15° (Figure 2a); (2) the Au NPs were placed in the same positions of condition (1), but the Au NPs were simulated by a cubic geometry (Figure 2b); (3) 40 spherical Au NPs were placed near the membrane, grouped in 8 clusters, each composed of 5 NPs with the geometry shown in Figure 2c. The shorter distance between the membrane and the NPs of each cluster was set equal to 60 nm, while the clusters were spaced with and angular distance equal to 45°. As a comparison, we analyzed a fourth condition in which the cell was exposed to time-varying electromagnetic fields but no Au NP was used. The three conditions "with NPs" and the one "no NP" condition were simulated when the cell was placed in two different positions, at distances d_1 = 0.05 mm and d_2 = 0.2 mm from the coil, for a total of eight conditions.

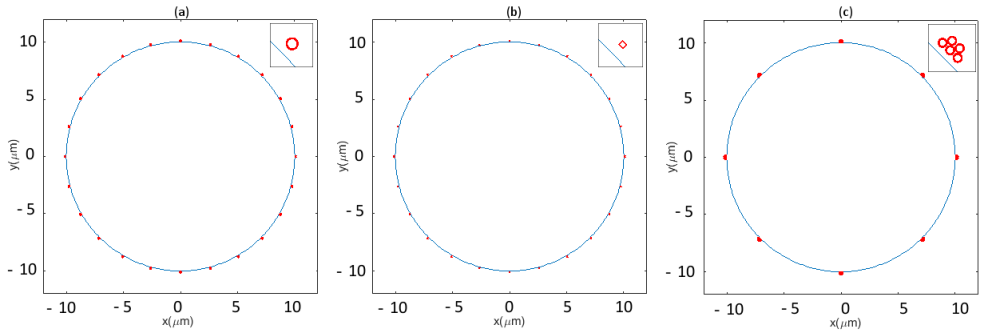

Figure 2. Schematic view of the three Au NP configurations around the cell: for each condition, the enlarged view of the NPs geometry is plotted in the upper right corner of the panel; (**a**) 24 spherical Au NPs placed at angular distance among them equal to 15°; (**b**) 24 cubic Au NPs placed at angular distance among them equal to 15°; (**c**) 40 spherical Au NPs grouped in 8 clusters, each composed of 5 NPs.

For all the eight considered conditions, the procedure involved two steps: first, the geometries shown in Figures 1a and 2 were simulated using the commercial software 5.6 COMSOL Multiphysics (AC/DC Module), the electric field induced by the time-varying magnetic field and enhanced by different geometries of Au NPs was evaluated, and the 99th percentile of the module of the electric field was calculated (see Section 2.2). Second, using the electric field calculated in the first step, a time-dependent simulation of the pore formation dynamics was carried out, following the procedure described in Section 2.3.

2.2. Evaluation of the Induced Electric Field

The 3D geometry consisting of the coil, the cell, and the Au NPs in different positions was simulated. The induced electric field was calculated by solving the electromagnetic problem under the Frequency Dependent Study application mode under the "Magnetic and Electric Field" solver of the AC/DC module in COMSOL.

The module of the electric field was evaluated in a cube with dimensions 25 × 25 × 25 µm centered around the cell, containing the extracellular medium and the nanoparticles. The 99th percentile of the module of the electric field was calculated on different volumes: on the whole cube under analysis, and, to consider the localized enhancement in proximity of each NP, in a 100 nm spherical neighborhood around each Au NP. In the case of the cluster of Au NPs, a 100 nm spherical neighborhood was considered around each NP, and the 99th percentile of the electric field was calculated on the union of the five spherical neighborhoods built around each NP.

Thus, for the 24 spherical and the 24 cubic Au NPs conditions, we calculated 25 values of electric field (99th percentiles calculated in each NP spherical neighborhood plus the one calculated on the whole box); for the clusters of Au NPs, we calculated 9 values of electric field (99th percentiles calculated in each cluster neighborhood plus the one calculated on the whole box); and for the "no NPs" condition, only the 99th percentile of the electric field on the whole box was calculated.

Among all these values, three parameters were considered for each simulation: $E^{99th}{}_{AllBox}$, corresponding to the 99th percentile of the electric field calculated on the whole cube, and $E^{99th}{}_{MAX}$ and $E^{99th}{}_{MIN}$, corresponding to maximum and minimum values, respectively, among those obtained calculating the 99th percentiles of the electric field in the spherical neighborhood around each Au NP.

2.3. Evaluation of Pore Dynamics

In order to evaluate the pore dynamics for the different Au NPs conditions, an approach similar to the one described in [25] was applied: a 2D geometry (see Figure 1b) was developed considering a spherical cell placed in an extracellular medium, represented by a square with dimensions of 40 µm × 40 µm. For each of the eight considered conditions,

three simulations were carried out, by applying as external electric potential to the high side of the square, modelled as positive anode electrode (Electrode 1 in Figure 1b), a cosine stimulus with frequency 33 kHz and amplitude equal to $V_{max} = E_{max} \times d$, where E_{max} was set equal to $E^{99th}{}_{ALLBOX}$, $E^{99th}{}_{MAX}$, and $E^{99th}{}_{MIN}$, calculated as described in Section 2.2, and d was the distance between the electrodes, equal to 40 µm. The electric potential on the low side of the square (Electrode 2 in Figure 1b) was set equal to zero in all the simulations, while the remaining sides of the square were modeled as insulating, thus obtaining an almost uniform electric field distribution, as shown in Figure 1c.

The time evolution and spatial distribution of the electric potential, $V(P,t)$, and of the pore density, $N(P,t)$, due to time-varying applied $E(t)$, are obtained by solving the following system of equations:

$$\begin{cases} \nabla \cdot \left(-\frac{\partial \epsilon \nabla V}{\partial t} - \sigma \nabla V - N i_{ep} \right) = 0 \\ \frac{\partial N}{\partial t} = \alpha e^{\left(\frac{V_m}{V_{ep}}\right)^2} \left(1 - \frac{N}{N_0} e^{-q\left(\frac{V_m}{V_{ep}}\right)^2} \right) \\ N(P,t) = 0 \; if \; P \notin cell \; membrane \end{cases}$$

where i_{ep} is the current in an aqueous pore [26], and $V_m = V_m$ (P^*, t) is the transmembrane potential in a generic point P^* on the external surface of the membrane, defined as the difference of electric potential in P^* and the electric potential in its geometric projection on the internal cell membrane boundary.

The second equation of the system is the asymptotic version of the Smoluchowski equation and describes the rate of creation and destruction of hydrophilic membrane pores per local membrane area N as a function of the V_m. Constant values V_{ep} = 258 mV, q = 2.46, α = 109, and $N_0 = 1.5 \times 10^9$ m^{-2} were adopted as in [26,27], being N_0 the "equilibrium value" of pore density when $V_m = 0$.

The phenomenon of pore creation is assumed to be activated at a fixed time instant t^* in a point P^*, when V_m reaches a critical value, i.e., $V_{crit} = 4V_{ep}$ = 1032 mV [24]. When the V_m reaches a value equal to or higher than V_{crit}, a fast variation occurs in the number of induced pores, making the pore density exceed the equilibrium ($N >> N_0$) with a very high time derivative [26].

All results were obtained by the Time-Dependent Study application mode under the "Electric Currents" solver of the AC/DC module in COMSOL.

The results are presented as a time evolution of the transmembrane voltage $V_m(P^*, t)$ and pore density $N(P^*, t)$ at a fixed point P^*, and in terms of variations of the conductivity along the cell membrane at a fixed point t^*.

3. Results

Figure 3 shows the 99th percentiles of the electric field module obtained for two different distances (d_1 and d_2) of the cell from the coil for the three different Au NP configurations considered, and, for a comparison, when no Au NP was used. As a first finding, a huge enhancement of the induced electric field was observed for both d_1 and d_2. For d_1, the observed values of $E^{99th}{}_{AllBox}$ were equal to 2580, 1955, and 1797 V/cm for the 24 spherical NPs, for the 24 cubic NPs, and for the 40 spherical NPs grouped in eight clusters, respectively, while when no Au NP was used, the 99th percentile of the module of the electric field was equal to 12.22 V/cm. When considering the enhancement in the neighboring of each NPs, a great difference was observed between NPs placed in different positions: in the spherical NP configuration, the maximum value of the 99th percentiles of the module of the electric field calculated around each NP, $E^{99th}{}_{MAX}$, was equal to 2959.2 V/cm, while the minimum $E^{99th}{}_{MIN}$ was equal to 36.938 V/cm. A higher difference was observed for the cubic NP configuration, were $E^{99th}{}_{MAX}$ and $E^{99th}{}_{MIN}$ were found to be equal to 3553.8 V/cm and 34.3 V/cm. Finally, when considering clusters of NPs, $E^{99th}{}_{MAX}$ and $E^{99th}{}_{MIN}$ were found to be equal to 1796.6 V/cm and 58.95 V/cm. For d_2, as expected, lower values were observed, but the presence of the Au NPs still caused a significant enhancement of the electric field: the observed values of $E^{99th}{}_{AllBox}$ were equal

to 924.26, 701.38, and 644.16V/cm for the 24 spherical NPs, for the 24 cubic NPs, and for the 40 spherical NPs grouped in eight clusters, respectively, while when no Au NP was used, $E^{99th}{}_{AllBox}$ was equal to 4.38 V/cm. Moreover, for d_2, a great difference was observed in the local enhancement of the electric field among NPs placed in different positions: $E^{99th}{}_{MAX}$ and $E^{99th}{}_{MIN}$ were found to be equal to 1059.9 and 13.786 V/cm for the spherical NP configuration, to 1276.5 and 12.25 V/cm for the cubic NP configuration, and to 811.4 and 42.5 V/cm for the 40 spherical NPs grouped in eight clusters.

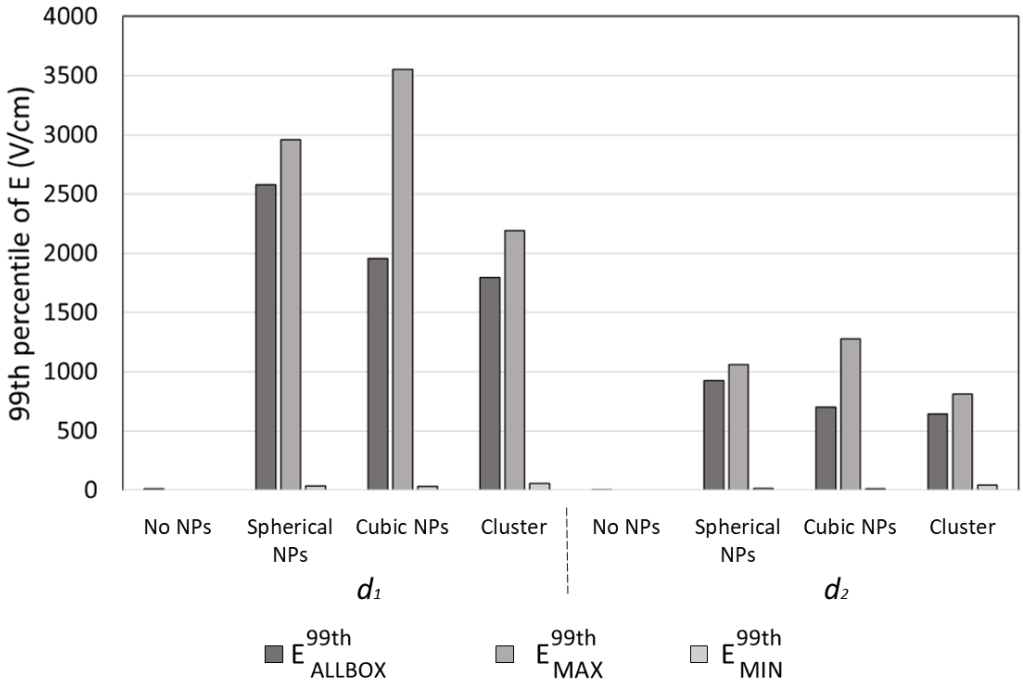

Figure 3. $E^{99th}{}_{AllBox}$, $E^{99th}{}_{MAX}$, and $E^{99th}{}_{MIN}$ at distances d_1 = 0.05 mm and d_2 = 0.2 mm from the coil for the three different Au NP configurations considered, and, for a comparison, when no Au NP was considered.

Figure 4 shows time evolution of the transmembrane voltage V_m and pore density N in three points of the cell membrane corresponding to θ equal to 0°, 45° and 90° (see Figure 1b), and the variation in the conductivity along the cell membrane for t equal to 15 µs when considering the amplitude of the external applied electric field equal to $E^{99th}{}_{AllBox}$, $E^{99th}{}_{MAX}$ and $E^{99th}{}_{MIN}$ for all the Au NP configurations when the distance between the cell and the coil was equal to d_1. An enlarged detail of the time evolution of the transmembrane voltage V_m is reported in Figure 4d,g,j, to highlight the effect of the pore dynamics on V_m. When no Au NP was considered, the transmembrane voltage V_m was not high enough to allow the pore opening in any point of the cell membrane (see Figure 4a–c).

For the spherical Au NP configuration (Figure 4d–f), when the amplitude of the external applied electric field was set to $E^{99th}{}_{AllBox}$ (red lines) and to $E^{99th}{}_{MAX}$ (gray lines), the time evolution of V_m was almost identical—in both cases, higher than the critical threshold assumed to enable pore opening for θ equal to 45° (dashed lines) and 90° (continuous lines). The corresponding time evolutions of the pore density N are shown in Figure 4e. As expected, the pore opening caused a sudden decrease in the time evolution of V_m (see the enlarged detail of Figure 4d). The membrane conductivity (Figure 4f) showed an important increase from the starting value of 1.26×10^{-7} to the maximum values equal to 1.12×10^{-3} S/m and 1.32×10^{-3} S/m, for $E^{99th}{}_{AllBox}$ (red lines) and $E^{99th}{}_{MAX}$ (gray lines), respectively, at arch lengths equal to 15.69 and 47.2 µm, corresponding to θ equal to 90° and 270°, i.e., at cell poles, while no increase was observed at arc length corresponding to θ equal to 0° and 180°. In addition to the significant increase corresponding to cell poles, membrane conductivity showed values higher than the starting value along a wide part of

the cell membrane, corresponding to θ values rising from 32° to 148° and from 212° to 328° for both $E^{99th}{}_{AllBox}$ (red lines) and $E^{99th}{}_{MAX}$ (gray lines), respectively, meaning that a large part of the cell membrane was permeabilized. When the amplitude of the external applied electric field was set equal to $E^{99th}{}_{MIN}$, i.e., to the minimum among the 99th percentiles values obtained in the neighborhood of the NPs, no pore opening was enabled at any point along the cell membrane.

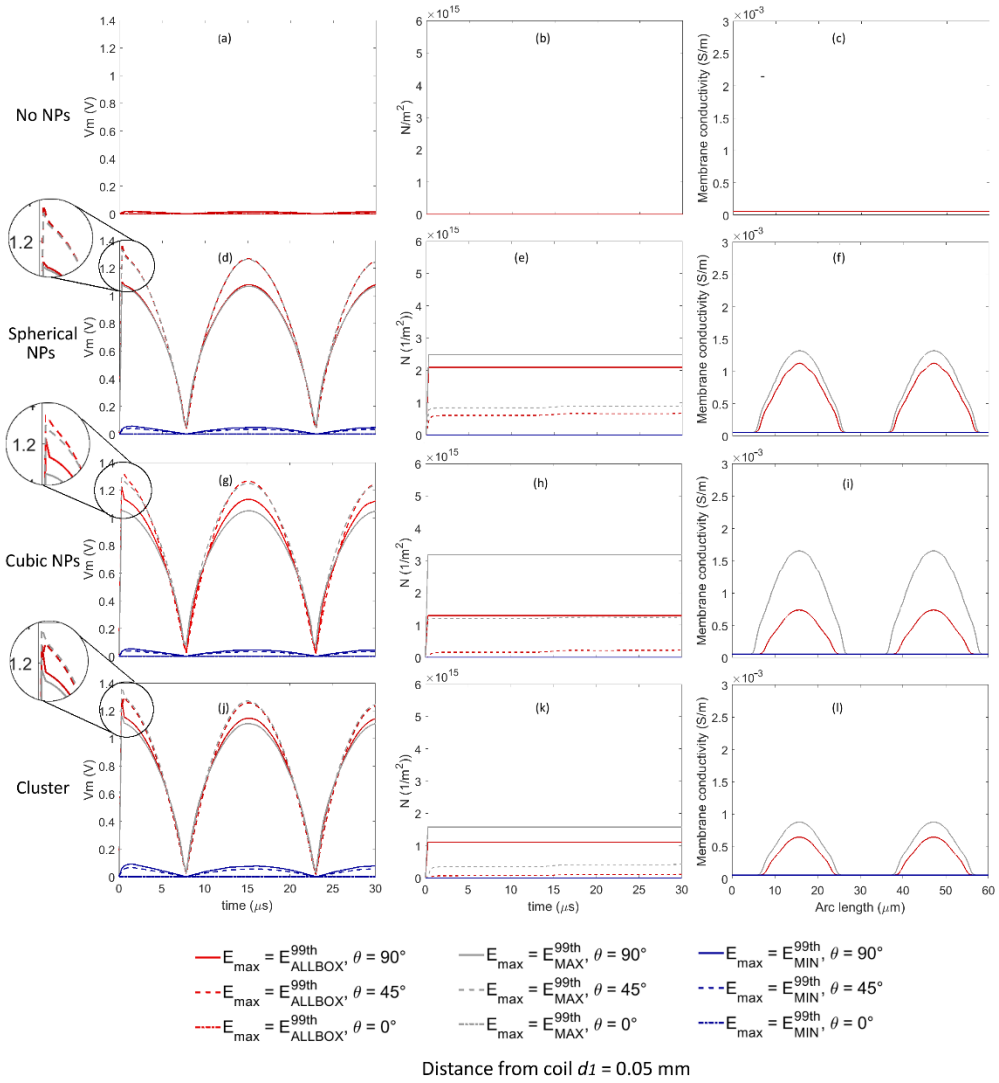

Figure 4. Time evolution of the transmembrane voltage V_m (first column, (**a**,**d**,**g**,**j**)), pore density N (second column, (**b**,**e**,**h**,**k**)), and the variation in the conductivity along the cell membrane for t equal to 15 μs (third column, (**c**,**f**,**i**,**l**)) at distance d_1 from the coil, when the amplitude of the external applied electric field was equal to $E^{99th}{}_{AllBox}$, $E^{99th}{}_{MAX}$, and $E^{99th}{}_{MIN}$, when no Au NP was considered (first row, (**a**–**c**)), and for the spherical, cubic, and cluster Au NP configurations (second row, (**d**–**f**), third row, (**g**–**i**), and fourth row, (**j**–**l**), respectively).

For the cubic Au NP configuration (Figure 4g–i), the time evolution of V_m was slightly different when the amplitude of the external applied electric field was set equal to $E^{99th}{}_{AllBox}$ (red lines) and to $E^{99th}{}_{MAX}$ (gray lines). In both cases, V_m was high enough to enable pore opening both for θ equal to 45° (dashed lines) and 90° (continuous lines), with higher pore density values for $E^{99th}{}_{MAX}$ than for $E^{99th}{}_{AllBox}$ (Figure 4h), and a corresponding decrease in the time evolution of V_m (enlarged detail of Figure 4g), with a sharper shape for θ equal to 90° (continuous lines) than for θ equal to 45° (dashed lines). The membrane conductivity (Figure 4i) showed an important increase from the starting value of 1.26×10^{-7} to the maximum values equal to 0.74×10^{-3} S/m and 1.65×10^{-3} S/m, for $E^{99th}{}_{AllBox}$ (red

lines) and $E^{99th}{}_{MAX}$ (gray lines), respectively, at arch lengths equal to 15.69 and 47.2 µm, corresponding to θ equal to 90° and 270°, i.e., at cell poles. Even if no increase was observed for θ equal to 0° and 180°, the variation in the conductivity along the cell arc length indicated that a large portion of the membrane, corresponding to θ rising from 27° to 153° and from 207° to 333° for $E^{99th}{}_{MAX}$ (gray lines), and to θ rising from 41° to 139° and from 229° to 311° for $E^{99th}{}_{AllBox}$ (red lines), was interested by pores opening. When the amplitude of the external applied electric field was set equal to $E^{99th}{}_{MIN}$, no pore opening was enabled at any point along the cell membrane.

For the spherical Au NPs grouped in clusters (Figure 4j–l), results were similar to those obtained for the spherical NPs (Figure 4d–f), with a similar time evolution of V_m for $E^{99th}{}_{AllBox}$ to $E^{99th}{}_{MAX}$: in both cases, V_m was high enough to enable pore opening both for θ equal to 45° (dashed lines) and 90° (continuous lines), with higher pore density values for $E^{99th}{}_{MAX}$ than for $E^{99th}{}_{AllBox}$ (Figure 4k), and a corresponding decrease in the time evolution of V_m (enlarged detail of Figure 4j), with a sharper shape for θ equal to 90° (continuous lines) than for θ equal to 45° (dashed lines). The membrane conductivity (Figure 4l) showed an increase from the starting value of 1.26×10^{-7} to the maximum values equal to 0.64×10^{-3} S/m and 0.89×10^{-3} S/m for $E^{99th}{}_{AllBox}$ (red lines) and $E^{99th}{}_{MAX}$ (gray lines), respectively, in correspondence of θ equal to 90° and 270°. Even if no increase was observed for θ equal to 0° and 180°, the variation in the conductivity along the cell arc length indicated that a large portion of the membrane, corresponding to θ rising from 36° to 144° and from 224° to 316° for $E^{99th}{}_{MAX}$ (gray lines), and to θ rising from 45° to 135° and from 225° to 315° for $E^{99th}{}_{AllBox}$ (red lines), was interested by pores opening. When the amplitude of the external applied electric field was set equal to $E^{99th}{}_{MIN}$, no pore opening was enabled at any point along the cell membrane.

Analogously to Figures 4 and 5 shows the time evolution of the transmembrane voltage V_m, the pore density N, and the variation in the conductivity along the cell membrane for t equal to 15 µs when considering the amplitude of the external applied electric field equal to $E^{99th}{}_{AllBox}$, $E^{99th}{}_{MAX}$, and $E^{99th}{}_{MIN}$ for all the Au NP configurations when the distance between the cell and the coil was equal to d_2. An enlarged detail of the time evolution of the transmembrane voltage V_m is reported in Figure 5d,g,j, to highlight the possible effect of the pore dynamics on V_m. Similarly to previous findings about d_1, also for d_2, when no Au NP was considered (Figure 5a–c), the transmembrane voltage V_m was not high enough to allow the pore opening at any point on the cell membrane.

When considering the spherical Au NP configuration (Figure 5d–f), only when the amplitude of the external applied electric field was set equal to $E^{99th}{}_{MAX}$, the V_m values were high enough to enable pore opening for θ equal to 90° (continuous gray line), while when the amplitude of the external applied electric field was set equal to $E^{99th}{}_{AllBox}$, V_m values were comparable to the critical threshold for pore opening for θ equal to 90°, enabling a slow increase in pore density (Figure 5e). This behavior is highlighted in the enlarged detail of Figure 5d: a slight decrease in V_m due to pore opening was observed only for $E^{99th}{}_{MAX}$ and for θ equal to 90° (continuous gray line). The membrane conductivity (Figure 5f) showed an increase from the starting value of 1.26×10^{-7} to the maximum values equal to 8.2×10^{-5} S/m and 0.19×10^{-3} S/m for $E^{99th}{}_{AllBox}$ (red lines) and $E^{99th}{}_{MAX}$ (gray lines), respectively, at arch lengths equal to 15.69 and 47.2 µm, corresponding to θ equal to 90° and 270°, i.e., at cell poles. The variation in the conductivity along the cell arc indicated that the portion of the membrane corresponding to θ rising from 65° to 115° and from 245° to 295° for $E^{99th}{}_{MAX}$ (gray lines), and to θ rising from 75° to 105° and from 255° to 285° for $E^{99th}{}_{AllBox}$ (red lines), was interested by pores opening. In all the remaining conditions, no pore opening was observed.

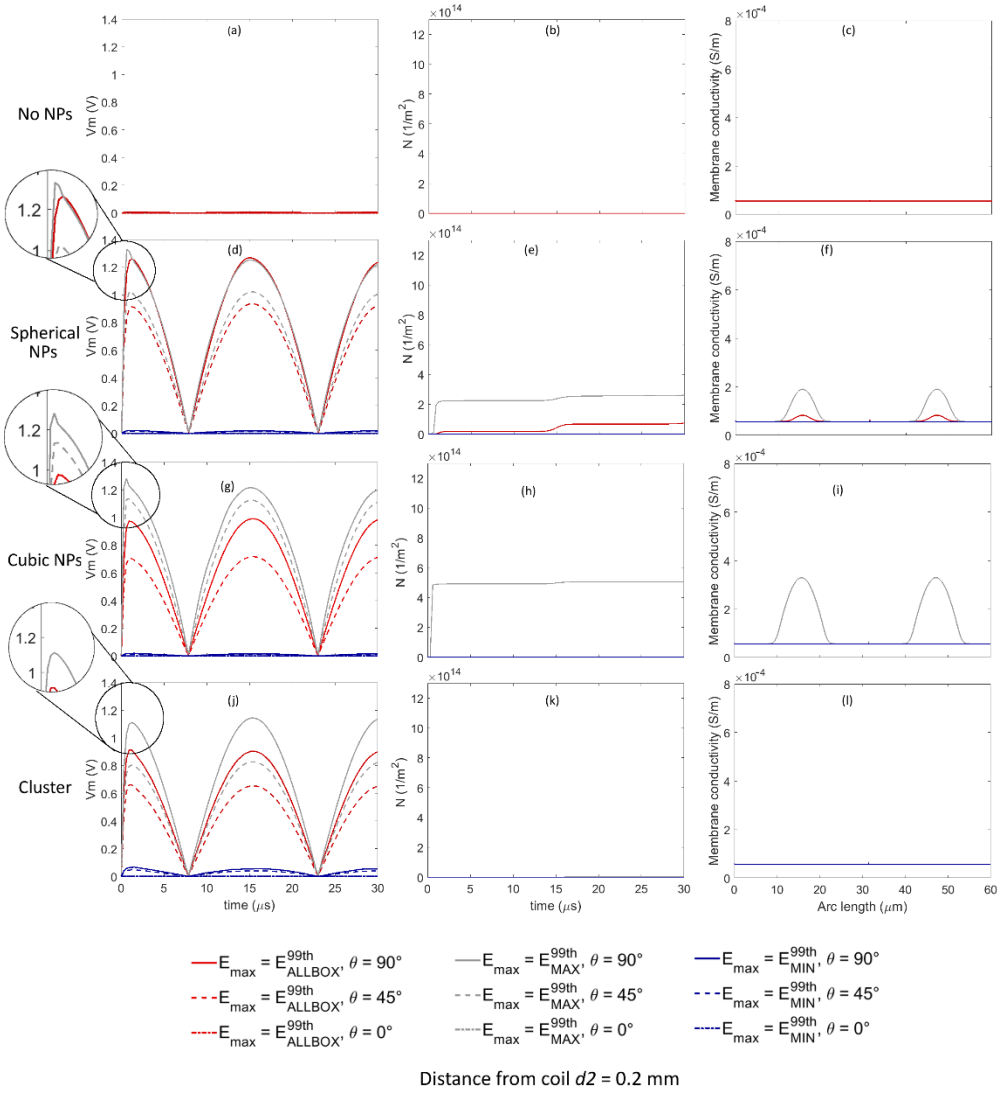

Figure 5. Time evolution of the transmembrane voltage V_m (first column, (**a**,**d**,**g**,**j**)), pore density N (second column, (**b**,**e**,**h**,**k**)), and the variation in the conductivity along the cell membrane for t equal to 15 µs (third column, (**c**,**f**,**i**,**l**)) at distance d_2 from the coil, when the amplitude of the external applied electric field was equal to $E^{99th}{}_{AllBox}$, $E^{99th}{}_{MAX}$, and $E^{99th}{}_{MIN}$, when no Au NP was considered (first row, (**a**–**c**)), and for the spherical, cubic, and cluster Au NP configurations (second row, (**d**–**f**), third row, (**g**–**i**), and fourth row, (**j**–**l**), respectively).

Moreover, for the cubic Au NP configuration (Figure 5g–i), only when the amplitude of the external applied electric field was set equal to $E^{99th}{}_{MAX}$, the V_m values were high enough to enable pore opening for θ equal to 90° (continuous gray line), while for θ equal to 45°, V_m values were comparable to the critical threshold for pore opening enabling a slow increase in pore density (Figure 5h). This behavior is highlighted in the enlarged detail of Figure 5g: a slight decrease in V_m due to pore opening was observed only for $E^{99th}{}_{MAX}$ and for θ equal to 90° (continuous gray line), while no decrease was observed in the other cases. The membrane conductivity for $E^{99th}{}_{MAX}$ (Figure 5f) showed an increase comparable to the values observed for d_1, ranging from the starting value of 1.26×10^{-7} to the maximum value equal to 0.33×10^{-3} S/m at arch lengths equal to 15.69 and 47.2 µm, corresponding to θ equal to 90° and 270°, i.e., at cell poles. The variation in the conductivity along the cell arc indicated that the portion of the membrane corresponding to θ rising from 53° to 127° and from 233° to 307° was interested by pores opening. In all the remaining conditions, no pore opening was observed.

Finally, when considering the spherical Au NPs grouped in clusters (Figure 5j–l), for none of the simulated conditions of position of the membrane was the pore opening mechanism enabled.

4. Discussion

This study focused on using a computational approach for the assessment of the electric field enhancement by using Au NPs in time-varying electromagnetic field cell membrane permeabilization, estimating the influence of the presence of Au NPs on trans-membrane potential and on the pore opening dynamics. The simulated conditions were based on the in vitro experimental set-up described by [18]. To account for variability and uncertainty about geometries and relative placement and aggregations of the Au NPs, three different configurations were considered: spherical Au NPs equally spaced around the cell; cubic Au NPs, for accounting for the possible edge effect, equally spaced around the cell; and spherical Au NPs grouped in clusters.

The experimental approach consisted of two steps: first, the electric field induced by the time-varying magnetic field and enhanced by different geometries of Au NPs was evaluated. As the enhancement of the electric field was greatly dependent on the position of the Au NPs with respect to the source, three values were considered: $E^{99th}{}_{AllBox}$, corresponding to the 99th percentile of the electric field calculated on a cube containing the Au NPs, and $E^{99th}{}_{MAX}$ and $E^{99th}{}_{MIN}$, corresponding to maximum and minimum values, respectively, among those obtained calculating the 99th percentiles of the electric field in 100 nm spherical neighborhood around each Au NP.

The results showed that when the cell and the Au NPs are placed very near to the coil, at distance d_1 = 0.05 mm, and when they are slightly further, at d_2 = 0.2 mm, a great enhancement of the electric field was obtained thanks to the presence of the NPs. When considering the $E^{99th}{}_{AllBox}$, the maximum increase due to the presence of the NPs was equal to about 21,000% for both d_1 and d_2 and was observed when simulating spherical NPs equally spaced around the cell. Comparing $E^{99th}{}_{AllBox}$ to $E^{99th}{}_{MAX}$ and $E^{99th}{}_{MIN}$, i.e., comparing the 99th percentile of the electric field obtained in the cube containing the Au NPs and the values obtained very near to the NPs, showed high variability. The maximum difference between $E^{99th}{}_{MAX}$ and $E^{99th}{}_{AllBox}$ was observed for the cubic NPs, as the $E^{99th}{}_{MAX}$ was 0.817 and 0.819 times greater than $E^{99th}{}_{AllBox}$ for d_1 and d_2, respectively, confirming previous findings about the edge effect and meaning that if a cubic Au NP was placed very near to the cell membrane, that specific point of the membrane would experience a very high electric field, thus enhancing the probability of pores opening. On the other hand, the maximum difference between $E^{99th}{}_{MIN}$ and $E^{99th}{}_{AllBox}$ was observed for the spherical NPs equally spaced around the cell, as between $E^{99th}{}_{AllBox}$ and $E^{99th}{}_{MIN}$, a decrement was observed almost equal to 98% for both d_1 and d_2.

While all these findings describe the enhancement of the electric field obtained when each Au NP is placed so far from the others that is not influenced by their presence, the influence of the relative positions of NPs placed at a short distance was simulated by considering 40 NPs grouped in eight homogeneous clusters. Interestingly, although the number of simulated NPs was higher, i.e., 40 NPs in the cluster configuration vs. 24 NPs in the equally spaced configuration, the $E^{99th}{}_{AllBox}$, $E^{99th}{}_{MAX}$, and $E^{99th}{}_{MIN}$ values in the cluster configuration were lower than those observed for the equally spaced spherical NPs. Although a direct comparison with values observed in literature is not possible, as no other study has focused on the use of NPs when considering time-varying magnetic fields for cell permeabilization, a similar result was observed in [24], where the authors found that if using Au NPs during electroporation protocol, the electric field enhancement was much higher for isolated NPs than for highly aggregated NPs.

All the considered configurations involved single NPs and grouped NPs equally spaced around and placed at very short distance, equal to 20 nm, from the cell membrane. To assess the influence of the distance from the cell membrane, two additional simulations considering the 24 spherical NPs placed at distances equal to 80 nm and 120 nm from

the cell membrane were carried out. The results showed that, as expected, the E field values found along the cell membrane decreased for greater distances: maximum E values obtained for distances of 80 nm and 140 nm were equal to 30% and 11%, respectively, of the value obtained for a distance equal to 20 nm. Similarly, mean E values for distances of 80 nm and 140 nm were found to be equal to 37% and 21%, respectively, of the value obtained for a distance equal to 20 nm. Of course, a drastic decrease in the amplitude of the electric field in proximity of the cell membrane would result in a decreased probability of pore opening. These results, well expected, confirmed that the proximity of the Au NPs to the cell membrane could play a key role in the local enhancement of the electric field, and thus in the probability of enable pore opening.

The second step in the experimental approach consisted of time-dependent simulation of the transmembrane potential and of the pore opening dynamic when a spherical cell was stimulated by the electric field induced by the time-varying magnetic field and enhanced by the presence of the Au NPs.

As a first finding, when no NPs were considered, the electric field values induced by the time-varying magnetic field were not high enough to cause the transmembrane potential V_m to overcome the critical threshold for pore opening, thus not enabling the cell membrane permeabilization, even if the cell was located at a small distance from the coil. This finding, well expected, was coherent with results by our previous study [19] and by other modelling studies [28,29], in which the authors found that with half-sinusoidal signals with frequencies lower than 500 MHz and amplitude equal to 5.5 T, the maximum V_m value was far below the critical value for pore opening.

When considering the enhancement due to the presence of NPs, the results were completely different: both for cells placed a distance of d_1 and d_2 from the coil, the presence of NPs enabled the cell permeabilization. As expected, a great difference in the transmembrane potential V_m and in the pore density was observed if considering $E^{99th}{}_{AllBox}$, $E^{99th}{}_{MAX}$, and $E^{99th}{}_{MIN}$. When the cell was placed in d_1, considering both $E^{99th}{}_{AllBox}$ and $E^{99th}{}_{MAX}$, the cell permeabilization in all the considered NP configurations was obtained preferentially at cell poles, while a wider area of permeabilization was obtained mainly when considering $E^{99th}{}_{MAX}$, i.e., when considering a very localized enhancement of the electric field, thus hypothesizing a very short distance between the cell membrane and Au NPs. This is coherent with findings of [20], in which the authors found that considering Au NPs during electroporation protocols shows strong increases in V_m with the presence of multiple NP clusters, demonstrating that enhanced pore opening could be possible even over sites far away from the poles, with proper distance between NPs cluster and cell membrane.

Finally, when the cell was placed in d_2, even if cell permeabilization was not achieved in all the considered NP configurations and not in all points of the membrane, Au NPs played a fundamental role in enabling pore opening in conditions in which, without them, it would be completely impossible to reach permeabilization.

Our findings—although not directly comparable with previously reported literature, as to our knowledge, no previous modeling study focused on the use of NPs when considering time-varying magnetic fields for cell permeabilization—were roughly in line with observations reported in studies about the use of Au NPs in electroporation protocols [20–24]. Moreover, our findings confirmed experimental findings reported in [18], in which authors found that conductive gold nanoparticles can significantly potentiate the permeabilizing effect of time-varying magnetic fields, with an increase in permeabilization from 1.57% with no NPs, to 10.99% using 20 nm Au NPs.

In conclusion, our study showed that the combined use of Au NPs and time-varying magnetic fields can significantly improve the permeabilization of cell membranes.

As the electric field induced in the cell suspension is not uniform, also due to the presence of nanoparticles in proximity of the membrane, the approach of applying an almost uniform electric field distribution to assess the pore dynamics used in this study could represent an important simplification of the phenomenon. However, this approach,

well established and already used in previous studies dealing with computational evaluation of pore dynamics influenced by electric fields distributions with [25] or without (see, e.g., [27]) the presence of nanoparticles near the cell membrane, allowed reducing the computational effort due to the presence of both nano-scale and millimeter-scale structures, while preserving the representativeness of the results.

The preliminary findings obtained in this study were encouraging and showed that the variability of NP geometries and configurations in proximity of the cell membrane had a strong influence on pore opening mechanisms. Future investigations should address all these aspects, and, due to the intrinsic variability and uncertainty characterizing a real in vitro experimental set, a stochastic dosimetry [30] approach, i.e., an innovative approach combining computational bioelectromagnetic and stochastic methods, could be used to obtain a realistic representation of the phenomena under study.

Moreover, in future studies, it would be interesting to investigate how different types of NPs, such as magnetic ones, could influence the permeabilization of the cell membrane, and to take into account not only the enhancement of the electric field, but also the role that different types of NPs could play in terms of the mechanical stress on the cell membrane locally induced by the magnetic and electric fields, which are hypothesized to play an important role in the permeabilization mechanism [19].

Author Contributions: Conceptualization, methodology, formal analysis, E.C., S.F. and M.P.; writing—original draft preparation, E.C., S.F. and M.P.; writing—review and editing, M.B. (Marta Bonato), S.G. and M.B. (Martina Benini). All authors have read and agreed to the published version of the manuscript.

Funding: This research received no external funding.

Institutional Review Board Statement: Not applicable.

Informed Consent Statement: Not applicable.

Data Availability Statement: The data presented in this study are available on request from the corresponding author.

Conflicts of Interest: The authors declare no conflict of interest.

References

1. Rems, L.; Miklavčič, D. Tutorial: Electroporation of cells in complex materials and tissue. *J. Appl. Phys.* **2016**, *119*, 201101. [CrossRef]
2. Miklavcic, D.; Rafael, V.D. Electrochemotherapy (ECT) and irreversible electroporation (IRE)-advanced techniques for treating deep-seated tumors based on electroporation. *Biomed. Eng. OnLine* **2015**, *14*, I1. [CrossRef]
3. Marty, M.; Sersa, G.; Garbay, J.R.; Gehl, J. Electrochemotherapy—An easy, highly effective and safe treatment of cutaneous and subcutaneous metastases: Results of ESOPE (European Standard Operating Procedures of Electrochemotherapy) study. *Eur. J. Cancer Suppl.* **2006**, *4*, 3–13. [CrossRef]
4. Fioretti, D.; Iurescia, S.; Fazio, M.M.; Rinaldi, M. In vivo DNA electrotransfer for immunotherapy of cancer and neurodegenerative diseases. *Curr. Drug Metab.* **2013**, *14*, 279–290. [CrossRef] [PubMed]
5. Lambricht, L.; Lopes, A.; Kos, S.; Sersa, G.; Préat, V.; Vandermeulen, G. Clinical potential of electroporation for gene therapy and DNA vaccine delivery. *Expert Opin. Drug Deliv.* **2016**, *13*, 295–310. [CrossRef] [PubMed]
6. Sardesai, N.Y.; Weiner, D.B. Electroporation delivery of DNA vaccines: Prospects for success. *Curr. Opin. Immunol.* **2011**, *23*, 421–429. [CrossRef] [PubMed]
7. Mahnič-Kalamiza, S.; Miklavčič, D. Scratching the electrode surface: Insights into a high-voltage pulsed-field application from in vitro & in silico studies in indifferent fluid. *Electrochim. Acta* **2020**, *363*, 137187.
8. Guenther, E.; Klein, N.; Mikus, P.; Stehling, M.K.; Rubinsky, B. Electrical breakdown in tissue electroporation. *Biochem. Biophys. Res. Commun.* **2015**, *467*, 736–741. [CrossRef]
9. Towhidi, L.; Firoozabadi, S.M.P.; Mozdarani, H.; Miklavcic, D. Lucifer Yellow uptake by CHO cells exposed to magnetic and electric pulses. *Radiol. Oncol.* **2012**, *46*, 119–125. [CrossRef]
10. Shankayi, Z.; Firoozabadi, S.M.P.; Mansurian, M.G. The Effect of Pulsed Magnetic Field on the Molecular Uptake and Medium Conductivity of Leukemia Cell. *Cell Biochem. Biophys.* **2013**, *65*, 211–216. [CrossRef]
11. Novickij, V.; Dermol, J.; Grainys, A.; Kranjc, M.; Miklavčič, D. Membrane permeabilization of mammalian cells using bursts of high magnetic field pulses. *PeerJ* **2017**, *5*, e3267. [CrossRef] [PubMed]

12. Novickij, V.; Grainys, A.; Lastauskienė, E.; Kananaviciute, R.; Pamedytytė, D.; Kalėdienė, L.; Novickij, J.; Miklavčič, D. Pulsed Electromagnetic Field Assisted in vitro Electroporation: A Pilot Study. *Sci. Rep.* **2016**, *6*, 33537. [CrossRef]
13. Novickij, V.; Girkontaite, I.; Zinkeviciene, A.; Svediene, J.; Lastauskiene, E.; Paskevicius, A.; Markovskaja, S.; Novickij, J. Reversible Permeabilization of Cancer Cells by High Sub-Microsecond Magnetic Field. *IEEE Trans. Magn.* **2017**, *53*, 1–4. [CrossRef]
14. Kardos, J.; Rabussay, D.P. Contactless magneto-permeabilization for intracellular plasmid DNA delivery in-vivo. *Hum. Vaccines Immunother.* **2012**, *8*, 1707–1713. [CrossRef] [PubMed]
15. Kranjc, S.; Kranjc, M.; Scancar, J.; Jelenc, J.; Sersa, G.; Miklavcic, D. Electrochemotherapy by pulsed electromagnetic field treatment (PEMF) in mouse melanoma B16F10 in vivo. *Radiol. Oncol.* **2016**, *50*, 39–48. [CrossRef] [PubMed]
16. Brezar, S.K.; Kranjc, M.; Čemažar, M.; Buček, S.; Serša, G.; Miklavčič, D. Electrotransfer of siRNA to Silence Enhanced Green Fluorescent Protein in Tumor Mediated by a High Intensity Pulsed Electromagnetic Field. *Vaccines* **2020**, *8*, 49. [CrossRef]
17. Heydarheydari, S.; Firoozabadi, S.M.; Mirnajafi-Zadeh, J.; Shankayi, Z. Pulsed high magnetic field-induced reversible blood-brain barrier permeability to enhance brain-targeted drug delivery. *Electromagn. Biol. Med.* **2021**, *40*, 361–374. [CrossRef]
18. Miklavcic, D.; Novickij, V.; Kranjc, M.; Polajzer, T.; Meglic, S.H.; Napotnik, T.B.; Romih, R.; Lisjak, D. Contactless electroporation induced by high intensity pulsed electromagnetic fields via distributed nanoelectrodes. *Bioelectrochemistry* **2019**, *132*, 107440. [CrossRef]
19. Chiaramello, E.; Fiocchi, S.; Bonato, M.; Gallucci, S.; Benini, M.; Parazzini, M. Cell Transmembrane Potential in Contactless Permeabilization by Time-Varying Magnetic Fields. *Comput. Biol. Med.* **2021**, *135*, 104587. [CrossRef]
20. Hu, Q.; Joshi, R.P. Continuum analysis to assess field enhancements for tailoring electroporation driven by monopolar or bipolar pulsing based on nonuniformly distributed nanoparticles. *Phys. Rev. E* **2021**, *103.2*, 022402. [CrossRef] [PubMed]
21. Zu, Y.; Huang, S.; Liao, W.-C.; Lu, Y.; Wang, S. Gold Nanoparticles Enhanced Electroporation for Mammalian Cell Transfection. *J. Biomed. Nanotechnol.* **2014**, *10*, 982–992. [CrossRef] [PubMed]
22. Huang, S.; Zu, Y.; Wang, S. Gold nanoparticle-enhanced electroporation for leukemia cell transfection. *Methods Mol. Biol.* **2014**, *1121*, 69–77.
23. Ghorbel, A.; Mir, L.M.; García-Sánchez, T. Conductive nanoparticles improve cell electropermeabilization. *Nanotechnology* **2019**, *30*, 495101. [CrossRef]
24. Movahed, S.; Li, D. Electrokinetic transport of nanoparticles to opening of nanopores on cell membrane during electroporation. *J. Nanopart. Res.* **2013**, *15*, 1511. [CrossRef]
25. Kaushik, A.; Nikkhah-Moshaie, R.; Sinha, R.; Bhardwaj, V.; Atluri, V.; Jayant, R.D.; Yndart, A.; Kateb, B.; Pala, N.; Nair, M. Investigation of ac-magnetic field stimulated nanoelectroporation of magneto-electric nano-drug-carrier inside CNS cells. *Sci. Rep.* **2017**, *7*, 45663. [CrossRef] [PubMed]
26. Neu, J.C.; Krassowska, W. Asympototic model of electroporation. *Phys. Rev. E* **1999**, *59*, 3471–3482. [CrossRef]
27. Lamberti, P.; Romeo, S.; Sannino, A.; Zeni, L.; Zeni, O. The role of pulse repetition rate in nsPEF-induced electroporation: A biological and numerical investigation. *IEEE Trans. Biomed. Eng.* **2015**, *62*, 2234–2243. [CrossRef]
28. Lucinskis, A.; Novickij, V.; Grainys, A.; Novickij, J.; Tolvaisiene, S.S. Modelling the cell transmembrane potential dependence on the structure of the pulsed magnetic field coils. *Elektron. Ir Elektrotech.* **2014**, *20*, 9–12. [CrossRef]
29. Hu, Q.; Joshi, R.P.; Miklavcic, D. Calculations of Cell Transmembrane Voltage Induced by Time-Varying Magnetic Fields. *IEEE Trans. Plasma Sci.* **2020**, *48*, 1088–1095. [CrossRef]
30. Chiaramello, E.; Fiocchi, S.; Parazzini, M.; Ravazzani, P.; Wiart, J. Stochastic Dosimetry for Radio-Frequency Exposure Assessment in Realistic Scenarios. In *Uncertainty Modeling for Engineering Application*; Springer: Cham, Switzerland, 2019; pp. 89–102.